Tailoring the properties of Y_2O_3 via synthesis parameters varied during the PVA-assisted sol-gel route

*J. C. C. Carvalho[1], G. F. C. Bispo[1], T. S. Lilge[2], C. S. Bezerra[2], A. B. Andrade[2], Z. S. Macedo[1,2], M. E. G. Valerio[1,2]**

[1]Federal University of Sergipe, Materials Science and Engineering Department, São Cristovão, SE, Brazil

[2]Federal University of Sergipe, Physics Department, Materials Preparation and Characterization Laboratory, 49100-000, São Cristovão, SE, Brazil

Abstract

The effect of synthesis parameters on the microstructural behavior and morphology during the yttrium oxide (Y_2O_3) formation is reported. Y_2O_3 crystals were produced by a modified sol-gel route assisted by polyvinyl alcohol solution varying the calcination temperature and solution pH. The crystalline phase formation was investigated using X-ray powder diffraction combined with the Rietveld refinement method. The microstructural properties were analyzed by using the Williamson-Hall formalism. The calcination temperature followed the thermal events observed in the differential thermal analysis combined with the thermogravimetric analysis of the precursor xerogel. It was seen that the combination of PVA and pH variation can be used to minimize the calcination time and temperature. The morphological analysis showed samples with different sizes and appearances depending on pH and calcination temperature. Therefore, it was shown that the parameters in the synthesis process can be used to tailor the properties of Y_2O_3, such as crystallite size, degree of structural ordering, and morphology, and consequently, improve the desired application.

Keywords: Y_2O_3, sol-gel method, thermal treatment, pH solution.

INTRODUCTION

The control of synthesis parameters has been of material science interest because they can change structure and morphology properties. For example, the particle size of compounds is susceptible to calcination parameters such as heating and cooling rate, plateau time, and pressure of synthesis [1]. Other features such as particle morphology depend on the synthesis method and pH solution besides synthesis conditions. All these parameters must be considered in the production of fine powders to enhance industrial applicability. However, most of the literature on material synthesis is worried only about the production of bulk without proper control of these parameters. For chemical synthesis, this can be troublesome since the pH of the solution plays an important role in the thermal events, phase formation, particle size, and particle morphology as well as luminescent properties [2, 3].

Yttria, Y_2O_3, is a well-known compound that has been attracting the attention of researchers due to its possible applications in sensors, optoelectronics devices, solar cells, anticancer activity, and lasers, among others [4-8]. As a yttria matrix, this material is commonly employed for incorporation of other rare-earth ions which present interesting optical properties and applications. For example, Nd-doped Y_2O_3 nanocrystals synthesized by sol-gel route were investigated for application in temperature sensing of biological systems [4]. In the literature, doped-Y_2O_3 nanoparticles have been synthesized via the PVA-assisted sol-gel method for employment in luminescence applications [9]. However, the influence of pH in the synthesis was not investigated. Results from the sol-gel route have shown an increase in the relative sensitivity as temperature sensing with the increase in crystallite size, indicating that the synthesis method can be employed for the control of optical parameters [4]. Another paper [10] shows that the crystallite size of Sm-doped Y_2O_3 changed with agitation conditions during the synthesis by the sol-gel method influencing the photoluminescence response. Also, undoped Y_2O_3, synthesized by the combustion process with different calcination temperatures, demonstrated the best response for application in low-dose X-ray conversion sensors due to the highest crystallite size [11]. Analyses of the pH effect in Bi-doped Y_2O_3 synthesized by the co-precipitation method reveal that changes in crystallite size and microstrain depend on pH variation [12].

Among the eco-friendly routes used for production, the following can be highlighted: sonochemical green synthesis [13], ultrasonic-microwave [14], microwave-hydrothermal [15], and coconut water-assisted sol-gel route [16]. Through the sol-gel route, it is possible to control the synthesis parameters and combine precursors for accelerating the chemical reactions during the process. The polyvinyl alcohol (PVA) content in oxides' synthesis influences the crystallization of materials [17], providing a route with OH

**megvalerio@academico.ufs.br*
https://orcid.org/0000-0003-1707-1078

groups that stabilize the metals in the polymer, thus reducing the precipitation of undesirable phases and the temperature to obtain the oxides. This paper presents the synthesis of undoped Y_2O_3 by a modified sol-gel method assisted by a PVA solution controlling the synthesis parameters. We pretend to produce Y_2O_3 varying two parameters: solution pH and calcination temperature. These parameters have demonstrated influence in particle morphology as well as microstructural deformations. The controlled synthesis can enable the industrial applicability of this route in the future.

EXPERIMENTAL

Y_2O_3 powders were synthesized via the sol-gel method assisted by polyvinyl alcohol (PVA) solution. The starting salts were yttrium nitrate [$Y(NO_3)_3$] and nitric acid (Alphatec, R.G.). PVA solution was prepared by dissolving PVA in distilled water at a concentration of 10% under magnetic stirring at 80 °C until the solution became homogeneous and transparent. Yttrium nitrate was dissolved in distilled water and PVA solution was dropwise added keeping a molar proportion of 2:1 [18]. A solution of HNO_3 (Neon, 65%) was used to adjust the initial pH value (~3) to approximately 0. The solution was heated and stirred at 150 °C for 2 h to obtain the gel phase. The sample was dried at 100 °C for 24 h, obtaining then a dried xerogel that was homogenized in an agate mortar. The calcination temperatures were estimated by using thermal analyses of xerogel. The differential thermal analysis (DTA) and thermogravimetry (TG) were performed from room temperature up to 1200 °C in a simultaneous system (SDT 2960, TA Instr.), with a heating rate of 10 °C/min under synthetic dry air flow. Based on the thermal analysis, the samples were calcined in an electric furnace with different plateau temperatures (600 and 1000 °C) for 1 h in an open atmosphere.

Structural analysis of the samples was performed using a conventional X-ray diffractometer (XRD, D8 Advanced, Bruker) with CuKα radiation, operating at 40 kV and 40 mA, over a 2θ range from 15° to 90° with steps of 0.02°. All measurements were carried out at room temperature and atmospheric pressure. The crystalline phases were identified by comparison using a standard XRD pattern from the Inorganic Crystal Structure Database (ICSD). In addition, Rietveld refinement was carried out using FullProf software [19] with the pseudo-Voigt function as the profile function. The refinement routine is described in detail in previous work [20]. From these analyses it was possible to investigate the crystallite size (D) and the microstructural deformation (lattice strain) by using the Williamson-Hall formalism [21]:

$$\beta.\cos\theta = \frac{k\lambda}{d} + 4\varepsilon.\sin\theta \qquad (A)$$

where k is the shape coefficient for the reciprocal lattice point (k=0.9 was used), λ is the X-ray wavelength, θ corresponds to the peak position of the identified crystalline phase, and D and ε are the effective crystallite size and the effective strain, respectively. The β represents the full width at half maximum (FWHM) of the diffraction peaks. The peak broadening was corrected by:

$$\beta = \sqrt{\beta_{exp}^2 - \beta_{inst}^2} \qquad (B)$$

where β_{exp}^2 and β_{inst}^2 are the broadenings of the measured line and the instrument, respectively [20]. β_{inst}^2 was determined from the XRD pattern of silicon powder standard by the angular dependence equation proposed by Caglioti et al. [22]. The profile parameters U=0.02806, V=-0.04376, and W=0.0292 were obtained from Rietveld refinement of silicon powder standard:

$$\beta = \sqrt{U.\tan^2\theta + V.\tan\theta + W} \qquad (C)$$

The morphology of the calcinated samples was analyzed through scanning electron microscopy (SEM, JSM-6510LV, Jeol). The microscope operated at 20 kV of accelerating voltage and the images were obtained at 5000x magnification.

RESULTS AND DISCUSSION

Firstly, thermal analyses were performed of Y_2O_3 xerogel before the calcination process. Fig. 1 shows the DTA/TG results of the Y_2O_3 xerogel. The curve analysis was divided into five different stages containing the main events. In the first stage, the mass loss from 100 to 200 °C was about 11%, and it was associated with loss of absorbed water by the xerogel. In the second stage, between 200 and 400 °C, a series of thermal events occurred associated with mass loss that was related to a breakdown of the PVA polymer chains and the loss of the organic matter [18, 23]. The thermal events in the TG curve above 400 °C were less evident. DTG (derivative of TG) curve showed an abrupt variation in the mass between 400 and 500 °C (third stage), accompanied by an exothermic peak associated with a large mass loss, at approximately 465 °C. This event may be related to the decomposition of PVA and precursor salts [18]. The fourth stage occurred at around 600 °C, where it was possible to observe an exothermic event, that can be associated with the

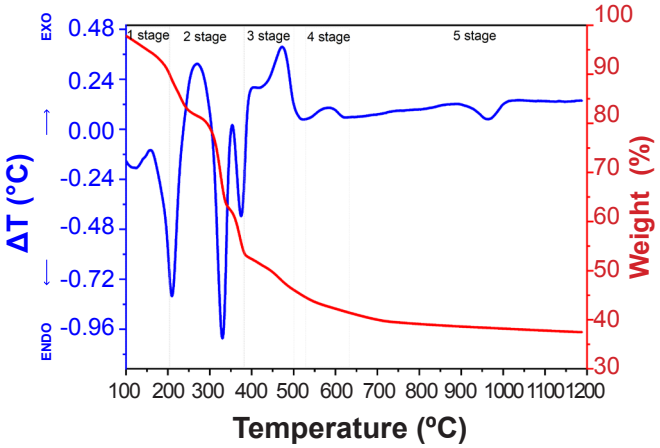

Figure 1: DTA and TG curves of the yttrium oxide precursor xerogel.

initial stage of the Y_2O_3 crystallization. Above 650 °C (fifth stage), there was no significant mass loss, indicating that the crystallization process was concluded and the increasing of the temperature could act only for a full ordering of the crystal lattice. The endothermic event observed in the DTA curve between 700 and 900 °C can be associated with the ordering of the crystal lattice or due to a structural change in Y_2O_3. Since Y_2O_3 requires some special thermodynamic conditions like very high temperature and high pressure to produce structural changes [24], this last possibility was overruled.

Fig. 2a shows the XRD patterns of the Y_2O_3 samples produced with the variation of pH solution and calcined at 600 and 1000 °C. The diffraction peaks were compared with the ICSD file 82420 for the Y_2O_3 phase of cubic structure and space group Ia-3 (206) [25]. The results showed that all samples present only this Y_2O_3 phase without the presence of additional phases. Another advantage compared with recent works which synthesized Y_2O_3 through the sol-gel method is the reduction of the time for 1 h of calcination in this present work. Several works report the Y_2O_3 formation with heat treatment above 2 h [26-29]. The time and temperature reduction for oxide crystallization using a PVA solution is discussed in the literature [18]. The PVA content in the synthesis process provides a route with OH groups that stabilize the metals in the polymer, thus reducing the precipitation of undesirable phases and the calcination temperature [17]. In the present work, in a solution containing nitrates, PVA could also have acted as a fuel, accelerating the process of materials formation during calcination [30]. However, fast nucleation can lead to disordering in the crystal lattice [31]. It was also possible to observe a narrowing effect in the width of diffraction peaks as the calcination temperature increased. This behavior can be attributed to either the crystallite size increase or microstrain, which could also contribute to the peak narrowing and displacement of the XRD patterns [25]. For better visualization, the main peak of the phase (plane 222) was highlighted for all samples and is presented in Fig. 2b. In addition to peak broadening for samples calcined at 600 °C, a shift in this peak can also be seen, which was dependent on the solution pH. For the sample with pH~0, a shift to smaller angles was observed, while for the less acidic pH, the opposite occurred, for larger angles. As can be seen, the temperature is an important parameter for Y_2O_3 production because it directly interferes with crystallization processes, since at 1000 °C, the XRD pattern corresponded to the reference pattern. Therefore, these structural effects were closely linked to the synthesis parameters for the material preparation such as those used in this work: heat treatment or pH variation. To investigate the effects in the Y_2O_3 crystal lattice ordering, the lattice parameters were determined by using Rietveld refinement applied to the raw XRD data. The structural parameters obtained from Rietveld refinement for the Y_2O_3 samples, such as cell parameters, unit cell volume, and agreement factors are shown in Table I and compared to the literature data [25]. The values of lattice parameters found from the refined structure for the samples were similar to the ones reported by Maslen et al. [25] for single crystalline/microcrystalline Y_2O_3, except for the samples calcined at 600 °C. For these samples, highlighted for the sample produced at pH 3, the lattice parameter and unit cell volume were slightly higher than those observed for the samples calcined at the highest temperature. That is in agreement with the displacement of the diffraction peak position observed in Fig. 2b.

The microstrain (ε) contribution in the narrowing width of the XRD peaks and the crystallite size (D) for all the samples were calculated from the Williamson-Hall (W-H) formalism [21] and are shown in Table II. The W-H plot was done by plotting $\beta\cos\theta$ versus $\sin\theta$, and it was possible to find the crystallite size from the intercept with the vertical axis and the microstrain was given from the slope of the straight line (Fig. 3). The narrowing of XRD peaks associated to the

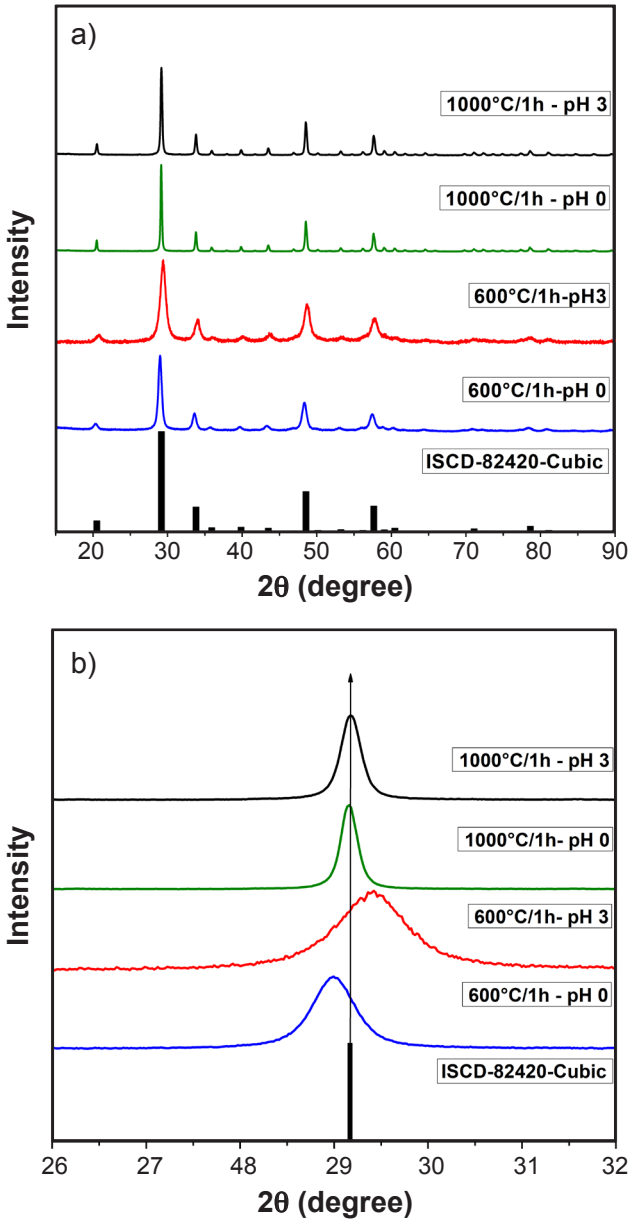

Figure 2: XRD patterns of Y_2O_3 synthesized at different parameters: a) general view; and b) expanded view of the diffraction peak (222).

Table I - Parameters for the Rietveld refinement of Y_2O_3 compared to the lattice parameters of ICSD file 82420.

Sample	χ^2	R_{Bragg} (%)	R_{WP} (%)	Lattice parameter a=b=c (Å)	Unit cell volume (Å^3)
600 °C - pH~0	2.26	5.33	11.9	10.6236(5)	1198.99(0.11)
600 °C - pH~3	1.67	6.20	16.8	10.6486(14)	1207.48(0.28)
1000 °C - pH~0	3.42	5.25	10.3	10.6061(1)	1193.08(0.03)
1000 °C - pH~3	2.84	4.87	8.74	10.6091(3)	1194.11(0.03)
Y_2O_3 [25]	-	-	-	10.5981(7)	1190.38

increase of crystallite size of samples synthesized by sol-gel route is discussed in the literature [32]. As can be seen in Table II, the broadening and the displacement observed in the XRD peak (Fig. 2b) were not only due to the structural microstrain. There was a combined effect of structural microstrain and crystallite size. The smaller calculated microstrain factor was found for the samples calcined at 1000 °C. These results meant that higher calcination temperatures could result in a coalescence of the crystallites with a subsequent increase of particle size, causing a better ordering in the crystal lattice, as observed in Table I by the relaxation in the unit cell volume of the Y_2O_3 unit cell. Now, comparing the results for changing the chemical environment differences can also be seen. The more acidic environment (pH~0), the faster the calcination process due to the interaction of PVA with HNO_3 ions (used to adjust the pH value). The sample synthesized at 1000 °C with pH 3 had the highest degree of structural ordering, which corroborated the XRD pattern (Fig. 2b) since fast nucleation can cause distortions in the structure. The pH of the solution influenced the crystallite size, in which there was a significant increase for the more acidic pH. It is reported in the literature that the highest crystallite size in Y_2O_3 particles is an important parameter for several applications, such as temperature sensing [4], down conversion properties [10], low-dose X-ray conversion sensors [11], and others. However, these works used longer times of calcination (from 2 to 5 h). Therefore, the pH variation can be used for improving the properties of Y_2O_3, consequently, the applications, besides minimizing the calcination time of Y_2O_3.

Fig. 4 shows the images for Y_2O_3 obtained by scanning electron microscopy. It was possible to visualize agglomerates for all samples, however with some differences. At the highest temperature (1000 °C), there was the begging of the spherical shape of particles, while at 600 °C, the small particles had an irregular assembly. Another difference observed was the

Table II - Microstrain factor (ε) and average crystallite size of Y_2O_3 samples.

Parameter	600 °C pH~0	600 °C pH~3	1000 °C pH~0	1000 °C pH~3
ε	0.0015	0.0019	0.0010	0.0002
D (nm)	20.1(5)	11.0(2)	115(3)	44(1)

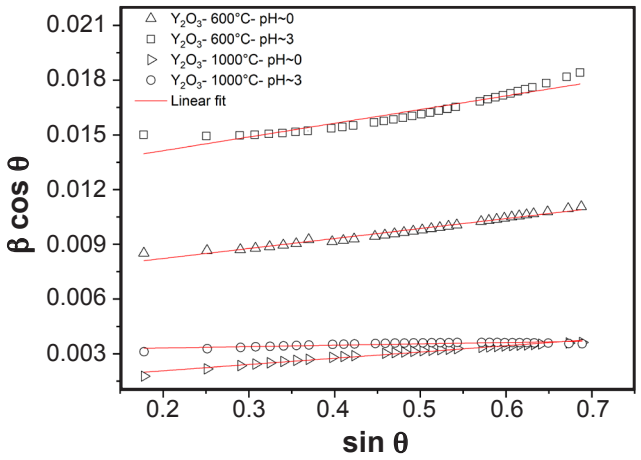

Figure 3: Williamson-Hall plot for Y_2O_3 samples.

particle size: samples calcined at 600 °C were smaller than those calcined at 1000 °C. A possible explanation is that the polymer chains covered the Y_2O_3 nuclei, limiting the reaction space and decreasing the contact between neighboring nuclei [18]. It was seen in the thermal analysis graph (Fig. 1) that the highest percentage of mass loss occurred up to approximately 600 °C. Above this temperature, stabilization occurred, which was associated with the material's crystallization process. Therefore, the sample calcined at 600 °C may have contained traces of organic matter and, consequently, influenced the morphology of the particles. The variation in morphology for Y_2O_3 has already been reported in the literature. The Y_2O_3 samples obtained by the sol-gel method with PVA without pH control have well-defined, coalesced spherical particles [9]. However, it should be considered that the samples were calcined at 1000 °C for 5 h, which probably favored the coalescence process. Another work [33] explored the Y_2O_3 produced by the sol-gel route and associated the change in morphology with the variation in parameters, such as starting acids and calcination temperature (800 and 1100 °C for 4 h) resulting in different shapes: needles, platelets, or spheres. The synthesis of Er-doped Y_2O_3 when changing the calcination temperature (600, 850, and 1000 °C for 5 h) was investigated for application in temperature sensing [29]. The authors found a dependence between the relative sensitivity with the particle size. However, in addition to using longer calcination times, neither of the works above explored the pH variation.

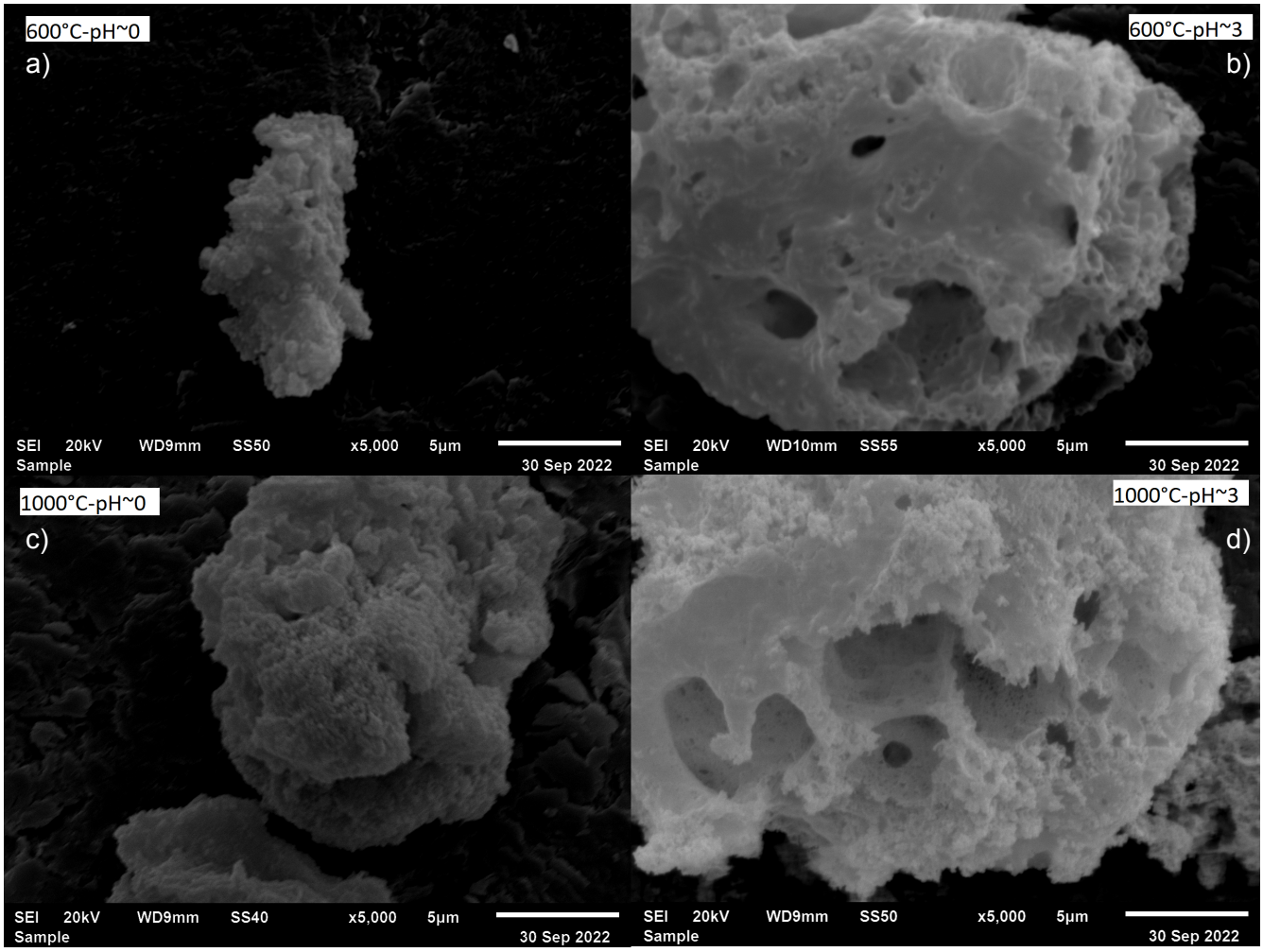

Figure 4: SEM images of Y_2O_3 particles synthesized at 600 °C (a,b) and 1000 °C (c,d) with pH~0 (a,c) and pH~3 (b,d)

As can see in Fig. 4, the pH variation also revealed differences in the morphology. The first one was the increase of the particles with the increase of pH (pH~3>pH~0). Another difference was the porosity appearance of the Y_2O_3 synthesized with pH~3. This behavior was visualized for both calcination temperatures. In the literature, the change in morphology and microstructure with the variation of precipitation agent when obtaining Y_2O_3 calcined for 3 h was investigated [34]. The authors observed a spongy morphology for particles containing NH_4OH as precipitating agent. The porosity behavior of particles of Y_2O_3 doped with Yb, Er, and Zn was investigated for application in a dye-sensitized solar cell (DSSC); this behavior increases the photovoltaic response of the Y_2O_3 used on TiO_2 photoanode [35]. The authors [36] noted a high porosity of the films, and this behavior is desirable because favors efficient diffusion of the dye in cells. Therefore, the calcination temperature and pH variation during the Y_2O_3 formation can be used for tailoring the desired application.

CONCLUSIONS

According to the results presented, it is concluded that the sol-gel route modified with PVA was satisfactory in the production of Y_2O_3 minimizing the time of calcination. The thermal analysis combined with XRD results showed that from 600 °C the crystalline phase of cubic Y_2O_3 was formed. The results obtained from Rietveld refinement combined with Williamson-Hall formalism showed that the synthesis parameters directly interfered with the crystallite size and structural deformation in the crystal lattice. There was a significant increase in the crystallite size for the more acidic pH (pH~0). As well as the structural properties, the morphology was also influenced by temperature and pH. Therefore, the control of the synthesis parameters is important because different kinds of Y_2O_3 particles can be produced and, thus, adjusting the properties according to the desired application.

ACKNOWLEDGMENTS

The authors gratefully acknowledge the CNPq, CAPES, FINEP, and FAPITEC-SE, Brazilian funding agencies, for financial support. Jéssica C. C. Carvalho also thanks to CNPq for the master in materials science and engineering scholarship (Edital 02/2016/COPES/POSGRAP/UFS).

This research used facilities of the Multiuser Centre for Nanotechnology at UFS (CMNano-UFS), a non-profit organization member of the National Multiuser Centres sponsored by Financiadora de Estudos e Projetos (FINEP). The CMNano technical staff is acknowledged for their assistance during the experiments under proposal number #008/2019.

REFERENCES

[1] C.S. Bezerra, A.B. Andrade, P.J.R. Montes, M.V.S. Rezende, M.E.G. Valerio, Opt. Mater. **72** (2017) 71.
[2] R. Thomatieli-Santos, M. Bernardi, A. Hernandes, J. Sol-gel Sci. Technol. **42** (2007) 173.
[3] D.F. Farias, C.M. de Abreu, S.M.V. Novais, Z.S. Macedo, J. Lumin. **194** (2018) 535.
[4] M.A. Gomes, I.S. Carvalho, L.F.A. Domingos, A.C.B. Silva, J.F.M. Avila, J.J. Rodrigues, M.A.R.C. Alencar, M.E.G. Valerio, Z.S. Macedo, Opt. Mater. **89** (2019) 536.
[5] D. Nunes, A. Pimentel, M. Matias, T. Freire, A. Araújo, F. Silva, P. Gaspar, S. Garcia, P.A. Carvalho, E. Fortunato, R. Martins, Nanomaterials **9**, 2 (2019) 234.
[6] S. Chen, J. Lin, J. Wu, Appl. Surf. Sci. **293** (2014) 202.
[7] P.C. Nagajyothi, M. Pandurangan, M. Veerappan, D.H. Kim, T.V.M. Sreekanth, J. Shim, Mater. Lett. **216** (2018) 58.
[8] J. Kong, D.Y. Tang, B. Zhao, J. Lu, K. Ueda, H. Yagi, T. Yanagitani, Appl. Phys. Lett. **86**, 16 (2005) 161116.
[9] G.A. Sobral, M.A. Gomes, J.F.M. Avila, J.J. Rodrigues, Z.S. Macedo, J.M. Hickmann, M.A.R.C. Alencar, J. Phys. Chem. Solids **98** (2016) 81.
[10] L. Lamiri, B. Kahouadji, M. Berd, A. Abdellatif, L. Benchallal, L. Guerbous, S. Ouhenia, A. Souici, L. Amiour, A. Zoukel, M. Samah, J. Rare Earths **41** (2023) 51.
[11] P. Praveenkumar, T. Subashini, G.D. Venkatasubbu, T. Prakash, Sens. Actuator A Phys. **297** (2019) 111544.
[12] E. Lee, J.J. Terblans, H.C. Swart, Vacuum **157** (2018) 237.
[13] N. Basavegowda, K. Mishra, R.S. Thombal, K. Kaliraj, Y.R. Lee, Catal. Lett. **147** (2017) 2630.
[14] J. Bi, L. Sun, Q. Wei, K. Zhang, L. Zhu, S. Wei, D. Liao, J. Sun, J. Mater. Res. Technol. **9**, 5 (2020) 9523.
[15] J. Kaszewski, B.S. Witkowski, L. Wachnicki, H. PrzybylÍnska, B. Kozankiewicz, E. Mijowska, M. Godlewski, J. Rare Earths **34**, 8 (2016) 774.
[16] M.A. Gomes, A.C.B. Silva, J.F.M. Avila, M.A.R.C. Alencar, J.J. Rodrigues, Z.S. Macedo, J. Lumin. **200** (2018) 43.
[17] J. Feng, T. Liu, Y. Xu, J. Zhao, Y. He, Y, Ceram. Int. **37**, 4 (2011) 1203.
[18] S.K. Saha, P. Pramanik, Nanostruct. Mater. **8**, 1 (1997) 29.
[19] J. Rodríguez-Carvajal, Physica B Condens. Matter **192**, 1 (1993) 55.
[20] A.B. Andrade, N. Ferreira, M.E.G. Valerio, RSC Adv. **7** (2017) 26839.
[21] G.K. Williamson, W.H. Hall, Acta Metall. **1**, 1 (1953) 22.
[22] G. Caglioti, A. Paoletti, F.P. Ricci, Nucl. Instrum. **3**, 4 (1958) 223.
[23] K.F. Suzart, A.B. Andrade, Z.S. Macedo, M.E.G. Valerio, J. Lumin. **203** (2018) 385.
[24] R. Dai, Z. Wang, Z. Zhang, Z. Ding, J. Rare Earths **28** (2010) 241.
[25] E. Maslen, V. Streltsov, N. Ishizawa, Acta Crystallogr. B Struct. Sci. Cryst. Eng. Mater. **52**, 3 (1996) 414.
[26] N. Wang, J. He, K. Ye, X. Song, T. Li, Infrared Phys. Techn. **93** (2018) 77.
[27] I. Benammar, R. Salhi, J.L. Deschanvres, R. Maalej, J. Mater. Res. Technol. **9**, 6 (2020) 12634.
[28] P.M. Kakade, A.R. Kachere, P.D. Sahare, A.V. Deshmukh, S.D. Dhole, S.R. Jadkar, N.T. Mandlik, J. Alloys Compd. **928** (2022) 167106.
[29] A.S. Laia, A.C.B. Silva, M.A. Gomes, Z.S. Macedo, M.E.G. Valerio, J.J. Rodrigues, M.A.R.C. Alencar, J. Alloys Compd. **926** (2022) 166816.
[30] M. Stoia, M. Barbu, M. Stefanescu, P. Barvinschi, L. Barbu-Tudoran, J. Therm. Anal. Calorim. **110**, 1 (2012) 85.
[31] T.S. Lilge, C.S. Bezerra, G.F.C. Bispo, A.B. Andrade, Z.S. Macedo, M.L. Moreira, M.E.G. Valerio, Dalton Trans. **49** (2020) 8540.
[32] M. Junaid, M.A. Khan, A. Majeed, H. Alkhaldi, M.S. Attia, M.A. Amin, M.A. Iqbal, Ceram. Int. **48**, 15 (2022) 21651.
[33] A. Dupont, C. Parent, B. Le Garrec, J.M. Heintz, J. Solid State Chem. **171**, 1 (2003) 152.
[34] E.E. Kaya, S. Gurmen, Physica E Low Dimens. Syst. Nanostruct. **115** (2020) 113668.
[35] F.L. Chawarambwa, T.E. Putri, S.H. Hwang, P. Attri, K. Kamataki, N. Itagaki, K. Koga, D. Nakamura, Opt. Mater. **123** (2022) 111928.
[36] M. Ahmad, D.A. Pandey, N. Rahim, Renew. Sust. Energy Rev. **77** (2017) 89.
(Rec. 14/11/2022, Rev. 27/12/2022, Ac. 07/01/2023)